nature nanotechnology

ARTICLES

PUBLISHED ONLINE: 24 APRIL 2011 | DOI: 10.1038/NNANO.2011.54

Enhanced magneto-optical effects in magnetoplasmonic crystals

V. I. Belotelov[1,2]*, I. A. Akimov[3,4]*, M. Pohl[3], V. A. Kotov[1,5], S. Kasture[6], A. S. Vengurlekar[6], Achanta Venu Gopal[6], D. R. Yakovlev[3,4], A. K. Zvezdin[1] and M. Bayer[3]

Plasmonics allows light to be localized on length scales much shorter than its wavelength, which makes it possible to integrate photonics and electronics on the nanoscale. Magneto-optical materials are appealing for applications in plasmonics because they open up the possibility of using external magnetic fields in plasmonic devices. Here, we fabricate a new magneto-optical material, a magnetoplasmonic crystal, that consists of a nanostructured noble-metal film on top of a ferromagnetic dielectric, and we demonstrate an enhanced Kerr effect with this material. Such magnetoplasmonic crystals could have applications in telecommunications, magnetic field sensing and all-optical magnetic data storage.

Surface plasmon polaritons (SPPs)—coupled oscillations of the electromagnetic field and the electron plasma in a metal—have an important role in plasmonics[1–5] because they allow electromagnetic energy to be concentrated in nanoscale volumes near metal/dielectric interfaces, which leads to the enhancement of Raman scattering[6,7] and other nonlinear optical effects. Including a magnetic material in a plasmonic structure would provide another means of control over the plasmons and the light in the device through magneto-optical effects[8] such as the Faraday effect (rotation of the polarization of transmitted light) and the Kerr effect (rotation of the polarization of reflected light). In particular, if the applied magnetic field is perpendicular to the plane of incidence of the light, the transverse magneto-optical Kerr effect (TMOKE) leads to a change in the intensity of the reflected light[8].

Magneto-optical effects in smooth films of ferromagnetic metals such as nickel are usually not large enough for device applications[8]. However, nanostructuring can increase the size of these effects by exploiting geometrical resonances rather than electronic ones[9–12], and plasmonic effects can lead to further increase. An applied magnetic field can alter the wave vector of an SPP on a smooth interface, but its transverse magnetic (TM) polarization will remain unchanged. An SPP-assisted increase in the TMOKE has been observed in smooth films of ferromagnetic metals such as nickel or iron[13–18], in smooth or perforated noble-metal/ferromagnetic-metal multilayers[19–23], in cobalt and iron gratings[24,25], in metal/semiconductor films[26], and in noble metals in high external magnetic fields[27]. An increase of the polar Kerr effect owing to localized surface plasmons has also been predicted for granular ferromagnetic composites[28].

The main disadvantage of most of these approaches is that the optical losses associated with the presence of a ferromagnetic metal are relatively high. Semiconductors and noble metals have the disadvantage that huge external fields (exceeding several tesla) are needed to observe magneto-optical effects comparable in size to those seen in ferromagnets.

Here, we combine nanostructuring and plasmonics in a structure that consists of a thin layer of a noble metal (gold) perforated with subwavelength slits on top of a smooth ferromagnetic dielectric (bismith iron garnet; Fig. 1). This structure offers a combination of a large Faraday rotation (owing to the ferromagnetic dielectric) and small optical losses for wavelengths longer than 650 nm (owing to the nanostructured noble metal). The cross-polarized transmission and polar Kerr rotation of a similar structure were recently measured as a function of external magnetic field[29]. Although the effects of plasmons on these processes were observed, enhancement of magneto-optical effects through SPPs was not demonstrated[29].

In previous theoretical work we have predicted that Faraday and Kerr effects can be resonantly increased in these structures, in particular near the Wood resonances[30,31]. Here, we confirm these predictions by observing significant enhancement of the TMOKE in transmission.

Surface magnetoplasmons and Wood anomalies

The TMOKE is usually characterized by the parameter δ, which is the relative change in the intensity of the light reflected by a medium when the magnetization $\mathbf{M}$ of the medium is reversed:

$$\delta = (R(\mathbf{M}) - R(-\mathbf{M})/R(0) \quad (1)$$

where R is the reflected light intensity. This change originates from a magnetic-field-induced change of the boundary conditions at the surface of the magnetic layer, and reaches a maximum value for an oblique incidence of p-polarized light (electric field vector $\mathbf{E}$ parallel to the plane of incidence), but almost vanishes for s-polarization ($\mathbf{E}$ perpendicular to the plane of incidence)[8]. For smooth ferromagnetic metals $\delta \approx 1 \times 10^{-3}$, which limits its usefulness for applications[8,32]. The TMOKE can also be detected in the light transmitted by a medium, but this effect is difficult to observe because it has an intrinsically small value and because light is only weakly transmitted through ferromagnetic metals[33]. Here, we concentrate on the observation of the TMOKE in magnetoplasmonic crystals in transmission.

In the absence of an external magnetic field, the magnetization $\mathbf{M}$ of the ferromagnetic film used in our experiments (see Methods) is perpendicular to the surface; an external magnetic field can be used

[1]A.M. Prokhorov General Physics Institute, Russian Academy of Sciences, 119991 Moscow, Russia, [2]M.V. Lomonosov Moscow State University, 119992 Moscow, Russia, [3]Experimentelle Physik 2, Technische Universität Dortmund, 44221 Dortmund, Germany, [4]A.F. Ioffe Physical-Technical Institute, Russian Academy of Sciences, 194021 St Petersburg, Russia, [5]V.A. Kotelnikov Institute of Radio Engineering and Electronics, Russian Academy of Sciences, 125009 Moscow, Russia, [6]Tata Institute of Fundamental Research, Mumbai, 400005, India. *e-mail: belotelov@physics.msu.ru; ilja.akimov@tu-dortmund.de

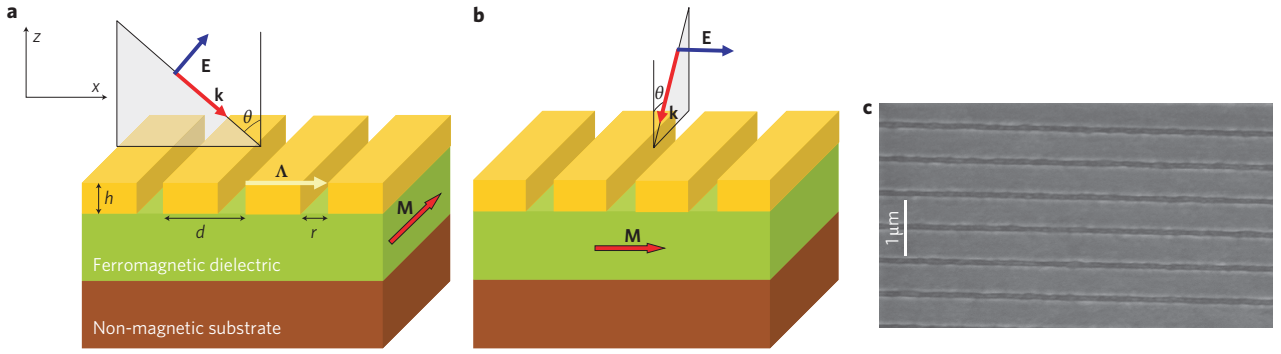

Figure 1 | Magnetoplasmonic heterostructures. a,b, A gold grating on top of a planar ferromagnetic dielectric (bismuth iron garnet film) grown on a non-magnetic substrate (gadolinium gallium garnet substrate). Two configurations are explored: with magnetization **M** in the ferromagnetic layer parallel to the slits, with the incident light p-polarized (**a**), and **M** perpendicular to the slits, with the incident light s-polarized (**b**). Dimensions of the gold layer: $d = 595$ nm, $r = 110$ nm, $h = 120$ nm (θ, angle of incidence). $\mathbf{\Lambda}$, **E** and **k** are defined in the text. **c**, Scanning electron micrograph of the gold grating.

to orient it either parallel to the slits in the gold layer of our samples (Fig. 1a) or perpendicular to these slits (Fig. 1b) The incident light is either p-polarized or s-polarized, and the plane of incidence is perpendicular to **M**.

Using a linear approximation for the dependence of the permittivity tensor describing the ferromagnetic film on the gyration (the magneto-optical parameter), this tensor is given by

$$\hat{\varepsilon}_{\mathrm{m}} = \begin{pmatrix} \varepsilon_2 & 0 & ig_y \\ 0 & \varepsilon_2 & -ig_x \\ -ig_y & ig_x & \varepsilon_2 \end{pmatrix} \tag{2}$$

where ε_2 is the dielectric function of the non-magnetized film, and g_x and g_y are the components of the gyration vector $\mathbf{g} = a\mathbf{M}$ (ref. 8). The magnetic tensor μ is taken to be unity, because the magnetic dipole response at optical frequencies is very weak[34].The gold metallic layer is characterized by the dielectric function ε_1 (ref. 35).

There are several vectors that characterize the optical and magneto-optical response of the system. These are the wave vector **k** and the electric field **E** of the incident light, and the lattice vector $\mathbf{\Lambda}$ (Fig. 1a). Together, they determine the necessary condition for the excitation of SPPs in the slit grating system $(\mathbf{E} \cdot \mathbf{\Lambda}) \neq 0$. They also determine the quasi-momentum of the SPPs $\mathbf{k}_{\mathrm{SPP}}$:

$$\mathbf{k} = \mathbf{k}_{\mathrm{SPP}} + (2\pi/d)m\mathbf{e}_x \tag{3}$$

where m is an integer and $\mathbf{e}_x$ is a unit vector along the x-axis. SPPs can be generated by p-polarized light in the configuration shown in Fig. 1a, and by s-polarized light in the configuration shown in Fig. 1b.

The necessary condition for the occurrence of the TMOKE is $[\mathbf{k} \times \mathbf{N}] \neq 0$ where **N** is the normal to the metal–dielectric interface. The cross product $[\mathbf{M} \times \mathbf{N}]$ is also very important. It is non-zero near the surface of the magnetized film. The magnetic field breaks the symmetry with respect to time reversal, whereas the interface breaks the space inversion, as does the **N** vector normal to it. Space–time symmetry breaking is characteristic of media with a toroidal moment $\boldsymbol{\tau}$, which has transformation properties similar to those of the cross product $[\mathbf{M} \times \mathbf{N}]$ (ref. 36). Consequently, the problem of SPP propagation along the interface of a transversely magnetized medium is similar to that of electromagnetic wave propagation in a bulk medium with a toroidal moment parallel to this direction. In electrodynamics, a toroidal moment is known to give rise to optical non-reciprocity, as manifested by a difference between the wave vectors for waves propagating forward and backward with respect to the toroidal moment[37]. An expression for the magneto-optical non-reciprocity for a smooth metal/magnetic–dielectric interface is given by[21,31,38]

$$\mathbf{k}_{\mathrm{SPP}} = \frac{\omega}{c}\sqrt{\frac{\varepsilon_1\varepsilon_2}{\varepsilon_1 + \varepsilon_2}}(1 + \alpha g_y) \tag{4}$$

where ω is the incident light frequency, c is the light velocity in vacuum, and $\alpha = (-\varepsilon_1\ \varepsilon_2)^{-1/2}\ (1 - \varepsilon_2^2/\varepsilon_1^2)^{-1}$.

The non-reciprocity effect is a prominent inherent feature of SPP-assisted TMOKE, as can clearly be seen for a smooth metal/dielectric interface. Far from the plasmonic resonance, one usually observes a monotonic, featureless reflection spectrum, and the TMOKE signal is quite small, even for metal ferromagnets. In contrast, at the SPP resonance, a pronounced dip appears in the reflection spectrum. Because the SPP wave vector differs for opposite magnetizations according to equation (4), the reflection dip shifts with magnetic field to smaller or higher frequencies and the TMOKE signal becomes enhanced by about an order of magnitude. In fact, in the frequency range of SPP generation, the TMOKE parameter δ is approximately equal to the product given by the frequency derivative of the reflection spectrum and the magnetic field induced frequency shift. Thus, TMOKE enhancement through SPPs occurs even for a smooth interface. However, there are drawbacks to this approach. First, to excite SPPs at the interface between a metal and a magnetic film (in the Kretschmann geometry), the refractive index of the prism must be larger than the refractive index of the magnetic film, which is rather difficult to achieve. Second, sputtering of the opaque metal layer onto the dielectric reduces the transmission to almost zero, preventing operation in transmission. This is why it might be worth considering a hybrid approach that involves a perforated metal.

Ebbesen *et al.*[39] demonstrated the phenomenon of extraordinary optical transmission in perforated metal films, where pronounced peaks appear in the transmission spectrum so that the structure is much more transparent than a smooth gold film. The SPPs in the periodic system are characterized by their quasimomenta k_{SPP} in the first Brillouin zone. It was shown that the Wood anomalies[40] (that is, the features in transmission and reflection spectra related to SPP excitation in metal gratings) are Fano resonances with a characteristic asymmetric profile with a maximum followed by a minimum (or vice versa)[41,42]. At such a resonance, the SPP frequencies do not exactly match those of the maximum and the minimum. The origin of the Fano shape is interference between resonant processes in the excitation of eigenmodes of the structure (such as quasi-waveguide modes, SPPs, slit modes and so on), plus a non-resonant contribution from the radiation directly scattered by the grating without excitation of eigenmodes.

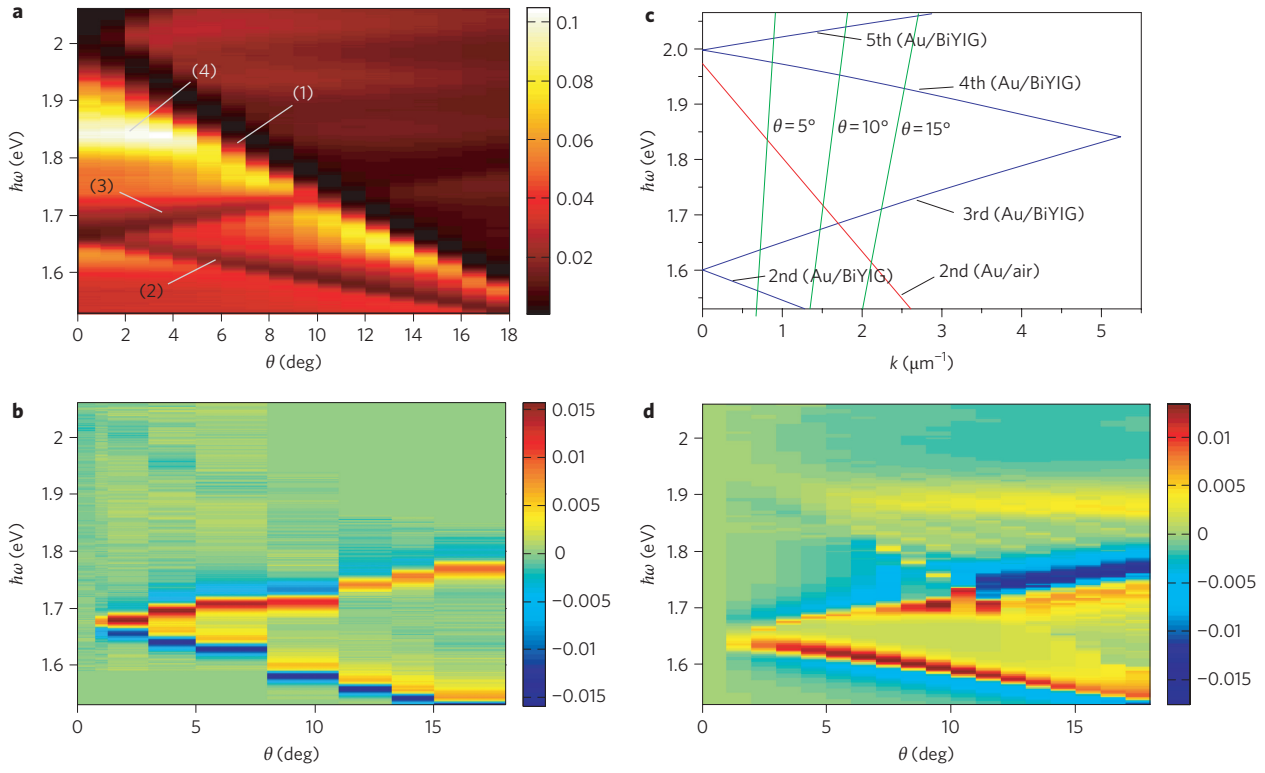

Figure 2 | Transverse magneto-optical Kerr effect (TMOKE). a, False-colour plot showing the transmission measured as a function of photon energy (vertical axis) and angle of incidence (horizontal axis). **M** is parallel to the slits and the incident light is p-polarized (as in Fig. 1a). The in-plane magnetic field strength is 2,000 Oe. Features (1)–(4) are related to SPPs or Fabry–Perot eigenmodes. **b**, False-colour plot showing the TMOKE parameter δ as a function of photon energy (vertical axis) and angle of incidence (horizontal axis). **c**, Dispersion diagram for SPPs at the gold/air interface (red line) and at the gold/iron-garnet interface (blue lines), calculated in the free lattice approximation within the first Brillouin zone; see text for more details. Green lines indicate dispersion curves for free-space photons for $\theta = 5°$, 10° and 15°. **d**, False-colour plot showing calculated values of TMOKE parameter δ.

Because SPPs can propagate along both surfaces of the perforated metal film, two types of Fano resonances can be observed. However, it is only the bottom metal surface adjacent to the ferromagnetic layer that contributes significantly to the TMOKE. Consequently, we can assume that TMOKE enhancement around the two resonances will be significantly different, exhibiting a much larger enhancement factor for the SPPs on the bottom interface. Furthermore, contrary to uniform films, the optical properties of perforated metals are also governed by other eigenmodes and anomalies[43,44]. Indeed, transmission/reflection dips and peaks might also be owing to Rayleigh anomalies or Fabry–Perot resonances. Such diversity of optical phenomena usually leads to considerable difficulties in their interpretation. In this case, observation of the TMOKE can reveal the difference between various phenomena: for example, Rayleigh anomalies (sharp maxima in the reflection spectra of metallic gratings) are related to electromagnetic field singularities when one of the diffracted orders becomes tangential to the grating surface and are determined by the grating period, so it is not possible for the magnetization to have any influence on them. Moreover, anomalies caused by Fabry–Perot resonances inside the slits should not be very sensitive to the magnetization, because they are mainly determined by slit depth and width[43].

Giant TMOKE in transmission mode

Preliminary numerical modelling enabled us to design the sample, that is, determine the gold grating period, gold thickness and slit width, and to adjust the main SPP resonances to the wavelength range 650–850 nm. This range is most suitable for magneto-optical experiments on bismuth iron garnets, because the magneto-optical figure of merit given by the ratio of the specific Faraday rotation to the absorption is highest at ~750 nm. (See Methods for a description of the numerical modelling procedure.)

The zero-order transmission spectrum for the configuration in Fig. 1a is shown in Fig. 2a. Comparison with the calculated band structure (Fig. 2c) allows us to attribute the pronounced Fano resonance (1) to the Wood's anomaly of the second-band SPP at the air/gold interface ($m = 1$ in equation 3), whereas the Fano resonances (2) and (3) are related to the second- and third-band SPP at the gold/iron-garnet interface ($m = \pm 1$ in equation 3). Finally, the prominent transmission peak (4) is attributed to the collective Fabry–Perot cavity mode inside the slits.

The experimentally measured TMOKE parameter δ is defined in accordance with equation (1), but with the reflection coefficient replaced by the transmission coefficient (Fig. 2b). Outside the resonances, the absolute value of δ is very small, even less than the experimental sensitivity (which is $\sim 1 \times 10^{-3}$). On this background, pronounced positive (red) and negative (blue) peaks are observed at which δ reaches values up to 1.5×10^{-2}. The regions of enhanced TMOKE clearly correspond to the regions of SPP excitation at the gold/iron-garnet interface (compare Fig. 2a and b). Electromagnetic modelling for the non-resonant case gives $\delta = 2 \times 10^{-4}$ to 8×10^{-4}, depending on the wavelength. This implies a TMOKE enhancement factor at the SPP resonance relative to the non-resonant case of ~20–100. Compared with the uncovered iron garnet film ($\delta \approx 1 \times 10^{-5}$, as predicted by theory), the enhancement factor is even larger, up to 1×10^{3}. It should be noted that we used a magnetic film with a relatively small concentration of bismuth. For iron garnets of composition $Bi_3Fe_5O_{12}$, the specific Faraday rotation is ~6° at $\lambda = 630$ nm, which is 13 times larger than for our sample[8]. Because the δ-value is proportional to the gyration (and to the specific

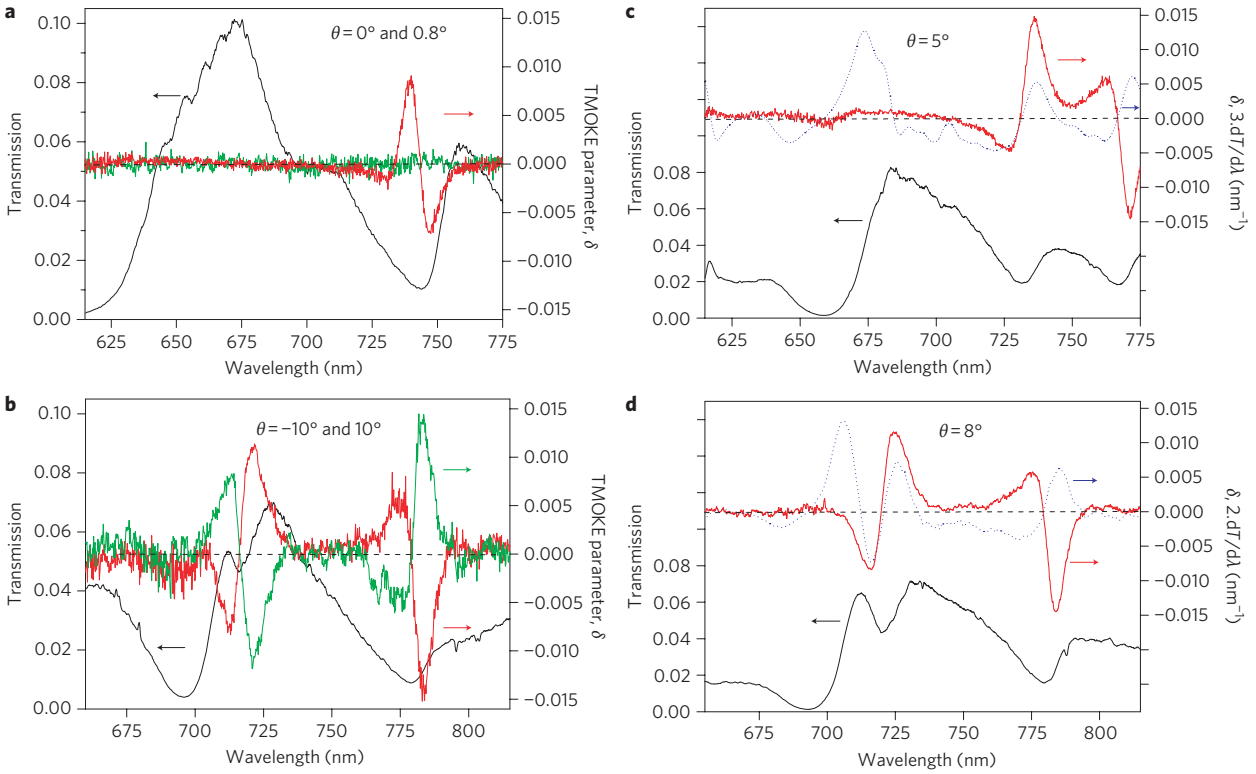

Figure 3 | Dependence of TMOKE on angle of incidence. a, Measured transmission (left axis) versus wavelength at normal ($\theta = 0°$) incidence (black), and TMOKE parameter δ (right axis) versus wavelength at normal incidence (green) and $\theta = 0.8°$ (red). (Transmission for $\theta = 0.8°$ is not shown.) **b**, Transmission (black) and δ (green) versus wavelength at $\theta = -10.0°$, and δ (red) versus wavelength at $\theta = 10.0°$. (Transmission for $\theta = 10.0°$ is not shown.) **c**, Transmission (black) and δ (red) versus wavelength at $\theta = 5.0°$. Blue line: derivative $dT/d\lambda$ (multiplied by a factor of 3), where T is transmission and λ is wavelength. **d**, Transmission (black), δ (red) and $dT/d\lambda$ (multiplied by factor of 2) versus wavelength at $\theta = 8.0°$. **M** is parallel to the slits and the incident light is p-polarized (as in Fig. 1a). The in-plane magnetic field strength is 2,000 Oe.

Faraday rotation), δ may exceed 0.2 by choosing an appropriate concentration of bismuth.

TMOKE as a tool for probing SPPs

A close-up of the TMOKE spectral shape is shown in Fig. 3. For normal incidence the TMOKE is zero (Fig. 3a). The magnetization-induced shift of the SPP resonance frequency vanishes and there is degeneracy of the SPPs travelling forwards and backwards. When **k** is not normal to the surface, the symmetry is broken and the degeneracy is lifted. SPP modes propagating in opposite directions are excited at slightly different frequencies, and the TMOKE appears. The value of δ reaches almost 1×10^{-2}, even if the incidence angle is as small as $\theta = 0.8°$ (Fig. 3a), in accordance with the Fano resonance for SPPs at the gold/iron-garnet interface in the vicinity of the Γ point of the first Brillouin zone. However, the transmission spectrum does not change notably on going from normal to slightly oblique incidence. This demonstrates the sensitivity of the TMOKE to the SPP modes in the structure. No measurable TMOKE signal is observed around the other features in the transmission spectrum (the peak at $\lambda = 675$ nm and the dip at $\lambda = 623$ nm), which is in agreement with the discussion above. This highlights the different sensitivity of the TMOKE to the excitation of different types of eigenmodes.

When the incidence angle becomes larger (for example, $|\theta| = 10°$, Fig. 3b), the excitation frequencies of the two SPPs propagating in opposite directions differ significantly, which gives rise to two well-resolved Fano resonances in transmission. The TMOKE accompanies both resonances, but with opposite signs of δ, reflecting the fact that these resonances are owing to SPPs propagating in opposite directions with respect to the cross product $[\mathbf{M} \times \mathbf{N}]$. This unravels another prominent feature of the TMOKE in magnetoplasmonic structures: through the sign of δ one can distinguish between resonances caused by SPPs propagating in opposite directions. Similar measurements for negative angles of incidence give the same value of δ but with opposite sign. This demonstrates that the observed effect is odd in magnetization and not an experimental artefact (Fig. 3b).

The values of δ for wavelengths close to the TMOKE resonances are comparable to the transmission derivative $dT/d\lambda$ (blue curves in Fig. 3c,d). This is in agreement with the discussion above, because the TMOKE enhancement is mainly owing to the magnetization-induced shift of the Fano resonances. It is instructive to recall here that the SPP excitation wavelengths coincide with neither peaks nor dips of the Fano resonances in transmission[41,42]. Figure 3c,d demonstrates that the TMOKE peaks do not exactly match the SPP frequencies, but coincide with the maxima and minima of $dT/d\lambda$ in the vicinity of the plasmonic resonances at the gold/iron-garnet interface. Other maxima and minima of $dT/d\lambda$ do not correspond to any peculiarities of the TMOKE, as they are related to the slopes of the transmission resonances caused by either SPPs on the top surface of the metal grating or by the cavity modes in the slits.

Above a certain incidence angle (for example, at $\theta = 15°$), the SPP resonance was barely detectable, but the considerable TMOKE still vividly indicates its frequency position (see peak (i) of δ in Fig. 4a).

The magnetic field dependence of δ is shown in Fig. 4b for the two main TMOKE peaks (i) and (ii) at $\theta = 15°$. At small magnetic fields the value of δ grows linearly with magnetic field, indicating that the in-plane component of the sample magnetization also has

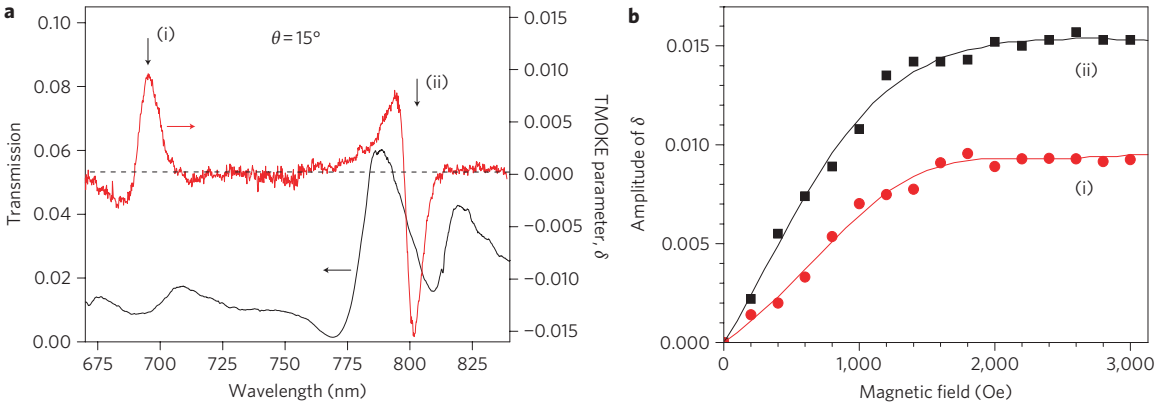

Figure 4 | Dependence of TMOKE on the magnetic field. a, Measured transmission (black curve; left axis) and TMOKE parameter δ (red curve; right axis) versus wavelength for $\theta = 15°$. **M** is parallel to the slits and the incident light is p-polarized (as in Fig. 1a). Two peaks can be clearly seen in the TMOKE spectrum. The in-plane magnetic field strength is 2,000 Oe. **b**, Amplitudes of the two peaks in the TMOKE spectrum in **a** as a function of magnetic field.

a linear dependence on magnetic field. Saturation takes place at a magnetic field strength of ~1,600 Oe, which is in good agreement with the predicted value of the effective uniaxial magnetic anisotropy field (see Methods). However, δ reaches relatively high values, even for smaller fields. For example, it is already 5×10^{-3} in a 300 Oe field.

Let us now consider the other possible transversal configurations. If in the configuration of Fig. 1a the light is s-polarized (rather than p-polarized), then no SPPs can be excited. It follows from the form of the tensor $\hat{\varepsilon}_m$ that if $\mu = 1$ then the TMOKE should also vanish. This corresponds to the 'non-plasmonic' and 'non-TMOKE' case (Table 1). The absence of the extraordinary peaks in Fig. 5 (curve T1) confirms this. If s-polarized light is incident along the slits (Fig. 1b) then SPPs are excited. However, no TMOKE is possible because of the s-polarization of light. So, here we are dealing with the 'plasmonic' and 'non-TMOKE' case (Fig. 5, curves T2 and δ2). Finally, if in the configuration of Fig. 1b the light is p-polarized, SPPs are not excited, but the TMOKE should be present. Thus we can label this situation 'non-plasmonic' and 'TMOKE', so that the TMOKE cannot be enhanced by SPPs. The absence of SPPs is clearly indicated by low transmission (Fig. 5, curve T3). It is not surprising that we are unable to measure a TMOKE signal, because the predicted value of δ (less than 1×10^{-4}) is too small to be detected with our experimental setup resolution. This case emphasizes the prominent role of SPPs for TMOKE enhancement.

Conclusions

We have fabricated a new magneto-optical material that consists of a smooth film of iron garnet (which is ferromagnetic), covered by a nanostructured layer of gold, and have shown how the excitation of SPPs in this magnetoplasmonic crystal affects its magneto-optical properties. Numerical calculations show that TMOKE parameter δ for a bare iron garnet film is very small ($\delta \approx 1 \times 10^{-5}$). When the film is covered by a smooth gold layer, the TMOKE can be resonantly enhanced up to $\delta \approx 5 \times 10^{-3}$ if the SPP is excited in the Kretschmann configuration, but it can be observed only in reflection because the transmission almost vanishes. However, when the gold layer is nanostructured, extraordinary optical transmission occurs and the value of δ can reach 1.5×10^{-2}. A unique property of the TMOKE in the transmission geometry is that the effect occurs mainly owing to the metal/magnetic dielectric interface and marginally depends on the bulk magnetization. We also demonstrate that the TMOKE is highly selective, because enhancement only occurs for the resonances related to the excitation of SPPs at the metal/magnetic dielectric interface. The TMOKE also changes sign for SPPs travelling in opposite directions, so it could become an important tool for the complete characterization of plasmonic nanostructures.

Although we have focused on the TMOKE, our previous work[30] leads us to believe that our magnetoplasmonic crystals could be used to enhance other magneto-optical effects such as the Faraday effect

Table 1 | The four different experimental configurations.

	p-polarized	s-polarized
M ∥ slits	SPP, TMOKE	(1) No-SPP, No-TMOKE
M ⊥ slits	(3) No-SPP, TMOKE	(2) SPP, No-TMOKE

In the present work the magnetization can be parallel or perpendicular to the slits, and the light can be s-polarized or p-polarized, leading to four different configurations. SPPs can be generated in two of these configurations, and TMOKE is also observed in two configurations. However, there is only one configuration in which SPPs are generated and TMOKE is observed together.

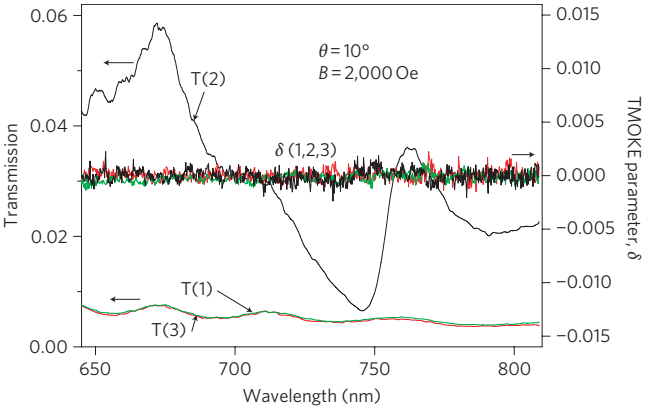

Figure 5 | Effect of different configurations. Measured transmission (left axis) and TMOKE parameter δ (right axis) versus wavelength for three of the four configurations described in Table 1. (Data for the fourth configuration are shown in Fig. 1a.) (1) **M** parallel to the slits; plane of incidence perpendicular to the slits; s-polarized light. Both the transmission and δ (both shown in red) have low values and are fairly featureless. (2) **M** perpendicular to the slits; plane of incidence along the slits; s-polarized light. The transmission spectrum (black) reaches high values and contains two pronounced peaks, and the value of δ (also in black) remains low. (3) **M** perpendicular to the slits; plane of incidence along the slits; p-polarized light. Both the transmission and δ (both shown in green) have low values and are fairly featureless.

and the polar and longitudinal Kerr effects. Potential applications of magnetoplasmonic crystals include plasmonic biosensors, magnetic field sensors and magnetic read heads. Moreover, recent results on the inverse Faraday effect[45] suggest that magnetoplasmonic crystals might also have applications in all-optical magnetic data storage devices operating at ultrafast (THz) frequencies.

Methods

Calculations. The electromagnetic modelling of transmission and TMOKE spectra was performed on the basis of the rigorous coupled waves analysis (RCWA) technique[46], extended to the case of gyrotropic materials[47]. Because the heterostructure is periodic, the electromagnetic field components in each layer can be represented as a superposition of Bloch waves. The Maxwell equations are written in a truncated Fourier space. The electromagnetic boundary conditions are then applied at the interfaces between the substrate region, the individual grating slabs and, finally, the upper surface of the structure. The sequential application of electromagnetic boundary conditions reduces the computing effort for the reflected and the transmitted diffracted field amplitudes to the solution of a linear system of differential equations. To improve convergence of the method we applied the correct rules of Fourier factorization introduced in ref. 47. Using this method we obtained satisfactory convergence for 41 diffraction orders.

Dispersion curves of the SPPs in Fig. 2c were obtained in the empty lattice approximation by folding the SPP dispersion curve for a smooth interface.

For the ferromagnetic film permittivity ε_2 and the absolute value of the gyration vector **g** we used our experimental data. Dispersion of both quantities was taken into account: for example, at $\lambda = 650$ nm, $\varepsilon_2 = 5.12 + 0.018i$ and $g = (3.4 + 0.4i) \times 10^{-3}$, and at $\lambda = 750$ nm, $\varepsilon_2 = 5.01 + 0.005i$ and $g = (1.9 + 0.2i) \times 10^{-3}$. For the permittivity of gold we took the experimental data from ref. 35.

Sample preparation. The magnetic layer of the magnetoplasmonic structure was a 2.5-μm-thick bismuth-substituted rare-earth iron garnet film with the composition $Bi_{0.4}(YGdSmCa)_{2.6}(FeGeSi)_5O_{12}$, grown by liquid phase epitaxy with a Bi_2O_3:PbO:B_2O_3 melt on a gadolinium gallium garnet $Gd_3Ga_5O_{12}$ substrate with orientation (111). The film had a uniaxial magnetic anisotropy and a maze-like domain structure. The stripe domain width was 2.4 μm and the Curie temperature 242 °C. The saturation magnetization of the film was $4\pi M_s = 453$ G and the bubble collapse field 238 Oe. The value of the effective uniaxial magnetic anisotropy field was $H_k^* = 1{,}600$ Oe, implying that application of an in-plane magnetic field with strength of 1,600 Oe leads to disappearance of the maze-like domain structure and results in a nearly complete in-plane magnetization orientation. The specific Faraday rotation was 0.46° per μm at a wavelength of 633 nm.

The magnetoplasmonic structure shown in Fig. 1 was fabricated by the following procedure. After initial cleaning of the iron garnet magnetic film in O_2 plasma, a gold layer was deposited on it using a thermal evaporation process. PMMA 950 e-resist was spin-coated on the gold layer at 3,000 r.p.m. and grating lines were drawn on the resist over an area of 1 mm^2 by electron-beam lithography (Raith e-Line), using the fixed beam moving stage technique. For large-area gratings, care should be taken to avoid stitching errors, edge distortion and the proximity effect, as well as ensuring vertical walls for the grooves. We optimized the aperture, write field, dose and acceleration voltage to obtain the envisioned grating parameters. We used a 10 μm aperture with a write field of 100 × 100 μm^2, a dose of 110 μC cm^{-2} and an acceleration voltage of 14 kV. The samples were then developed in methyl isobutyl ketone for 90 s at 21 °C followed by rinsing in isopropyl alcohol for 30 s. In the next step, the pattern was transferred to the metal by reactive ion etching using argon ion plasma. The dry etch process was carried out to first calibrate the etch rates of both PMMA and gold in Cl_2 and argon plasmas. The argon plasma process was found to be suitable for ensuring that there was no unpatterned gold under the gratings, and also to achieve the required grating depth. To obtain optimum grating parameters we used thicker resist (300 nm) and gold layers (140 nm). The etch process parameters were as follows: etch time, 7 min; flow rate, 50 s.c.c.m.; radiofrequency power, 135 W; chamber pressure, 0.2 Pa.

The sample was characterized by an atomic force microscope. The period and groove width were verified by scanning electron microscopy imaging. The following grating parameters were obtained: depth of grooves, 120 nm; period, 595 nm; air groove width, 110 nm.

Experimental setup and measurements. For magneto-optical measurements we used a tungsten halogen lamp as a source of white light with stability better than 0.1%. The light was first coupled into an optical fibre (core, 200 μm; numerical aperture, 0.22). The outcoming light from the fibre was then collimated with an achromatic lens (focal distance, 300 mm) and focused onto a sample using a second achromatic lens with the same focal distance. We used a 4-mm-diameter diaphragm between the lenses to reduce the maximum angle of the light cone to below 1°. The light was focused on the sample into a spot with diameter of ~300 μm. To perform measurements at different angles of light incidence, the sample was mounted on a rotation stage. The zero-order transmission signal was spectrally dispersed with a single monochromator (linear dispersion, 6.28 nm mm^{-1}) and detected with a charge-coupled device camera. The overall spectral resolution was below 0.3 nm. The polarization of the transmitted light was resolved by a polarizer in the detection path. The measured spectra were virtually identical if the polarizer was introduced in the excitation path, that is, before the sample. Magnetic fields up to 4 kOe were applied in transverse geometry using a water-cooled electromagnet. During measurements, the sample was kept at room temperature.

Received 11 January 2011; accepted 9 March 2011; published online 24 April 2011

References

1. Heber, J. Surfing the wave. *Nature* **461,** 720–722 (2009).
2. Polman, A. Plasmonics applied. *Science* **322,** 868–869 (2008).
3. Maier, S. (ed.) Special Issue: Plasmonics and nanophotonics *Phys. Stat. Sol. RRL* **4,** A85–A98, 241–297 (2010).
4. Bozhevolnyi, S. I. *Plasmonics Nanoguides and Circuits* (Pan Stanford, 2008).
5. Najafov, H., Lee, B., Zhou, Q., Feldman, L. C. & Podzorov, V. Observation of long-range exciton diffusion in highly ordered organic semiconductors. *Nature Mater.* **9,** 938–943 (2010).
6. Wurtz, G. A., Pollard, R. & Zayats, A. V. Optical bistability in nonlinear surface-plasmon polaritonic crystals. *Phys. Rev. Lett.* **97,** 057402 (2006).
7. Kneipp, K. Surface-enhanced Raman scattering. *Physics Today* 40–46 (November 2007).
8. Zvezdin, A. & Kotov, V. *Modern Magnetooptics and Magnetooptical Materials* (IOP, 1997).
9. Sarychev, A. K. & Shalaev, V. M. *Electrodynamics of Metamaterials.* (World Scientific, 2007).
10. Inoue, M., Arai, K., Fujii, T. & Abe, M. One-dimensional magnetophotonic crystals. *J. Appl. Phys.* **85,** 5768–5771 (1999).
11. Levy, M., Yang, H. C., Steel, M. J. & Fujita, J. Flat-top response in one-dimensional magnetic photonic bandgap structures with Faraday rotation enhancement. *Lightwave Technol.* **19,** 1964–1970 (2001).
12. Zvezdin, A. K. & Belotelov, V. I. Magnetooptical properties of photonic crystals. *Eur. Phys. J. B* **37,** 479–487 (2004).
13. Ferguson, P. E., Stafsudd, O. M. & Wallis, R. F. Surface magnetoplasma waves in nickel. *Physica B & C* **86–88,** 1403–1405 (1977).
14. Burke, J. J., Stegeman, G. I. & Tamir, T. Surface-polariton-like waves guided by thin, lossy metal films. *Phys. Rev. B* **33,** 5186–5201 (1986).
15. Hickernell, R. K. & Sarid, D. Long-range surface magnetoplasmons in thin nickel films. *Opt. Lett.* **12,** 570–572 (1987).
16. Olney, R. D. & Romagnoli, R. J. Optical effects of surface plasma waves with damping in metallic thin films. *Appl. Opt.* **26,** 2279–2282 (1987).
17. Newman, D. M., Wears, M. L. & Matelon, R. J. Plasmon transport phenomena on a continuous ferromagnetic surface. *Europhys. Lett.* **68,** 692–698 (2004).
18. Bonod, N., Reinisch, R., Popov, E. & Neviere, M. Optimization of surface-plasmon-enhanced magneto-optical effects. *J. Opt. Soc. Am. B* **21,** 791–797 (2004).
19. Gonzalez-Diaz, J. B. *et al.* Surface magneto-plasmon nonreciprocity effects in noble-metal/ferromagnetic heterostructures. *Phys. Rev. B* **76,** 153402 (2007).
20. Vila, E. F. *et al.* Surface plasmon resonance effects in the magneto-optical activity of Ag–Co–Ag trilayers. *IEEE Trans. Magn.* **44,** 3303–3306 (2008).
21. Temnov, V. *et al.* Active magnetoplasmonics in hybrid metal/ferromagnet/metal microinterferometers. *Nature Photon.* **4,** 107–111 (2010).
22. Clavero, C., Yang, K., Skuza, J. R. & Lukaszew, R. A. Magnetic-field modulation of surface plasmon polaritons on gratings. *Opt. Lett.* **35,** 1557–1559 (2010).
23. Armelles, G. *et al.* Magnetoplasmonic nanostructures: systems supporting both plasmonic and magnetic properties. *J. Opt. A* **11,** 114023 (2009).
24. Newman, D. M., Wears, M. L., Matelon, R. J. & Hooper, I. R. Magneto-optic behavior in the presence of surface plasmons. *J. Phys.: Condens. Matter* **20,** 345230 (2008).
25. Buchin, E. Y., Vaganova, E. I., Naumov, V. V., Paporkov, V. A. & Prokaznikov, A. V. Enhancement of the transversal magnetooptical Kerr effect in nanoperforated cobalt films. *Tech. Phys. Lett.* **35,** 589–593 (2008).
26. Aers, G. C. & Boardman, A. D. The theory of semiconductor magnetoplasmon-polariton surface modes: Voigt geometry. *J. Phys. C* **11,** 945–959 (1978).
27. Strelniker, Y. M. & Bergman, D. J. Transmittance and transparency of subwavelength perforated conducting films in the presence of a magnetic field. *Phys. Rev. B* **77,** 205113 (2008).
28. Zharov, A. A. & Kurin, V. V. Giant resonant magneto-optic Kerr effect in nanostructured ferromagnetic metamaterials. *J. Appl. Phys.* **102,** 123514 (2007).
29. Wurtz, G. A. *et al.* Controlling optical transmission through magneto-plasmonic crystals with an external magnetic field. *New J. Phys.* **10,** 105012 (2008).
30. Belotelov, V. I., Doskolovich, L. L. & Zvezdin, A. K. Extraordinary magnetooptical effects and transmission through the metal–dielectric plasmonic systems. *Phys. Rev. Lett.* **98,** 077401 (2007).
31. Belotelov, V. I., Bykov, D. A., Doskolovich, L. L., Kalish, A. N. & Zvezdin, A. K. Extraordinary transmission and giant magneto-optical transverse Kerr effect in plasmonic nanostructured films. *J. Opt. Soc. Am. B* **26,** 1594–1598 (2009).

32. Krinchik, G. S. & Artem'ev, V. A. Magneto-optical properties of Ni, Co and Fe in ultraviolet visible and infrared parts of spectrum. *J. Exper. Theor. Phys.* **26,** 1080–1085 (1968).
33. Druzhinin, A. V., Lobov, I. D., Mayevskiy, V. M. & Bolotin, G. Transverse magnetooptical Kerr effect in transmission. *Phys. Met. Metallogr.* **56,** 58–65 (1983).
34. Landau, L. D. & Lifshitz, E. M. *Electrodynamics of Continuous Media* (Pergamon, 1984).
35. Johnson, P. B. & Christy, R. W. Optical constants of the noble metals. *Phys. Rev. B* **6,** 4370–4376 (1972).
36. Dubovik, V. M. & Tosunyan, L. A. Toroidal moments in the physics of electromagnetic and weak interactions. *Sov. J. Part. Nucl.* **14,** 504–519 (1983).
37. Kalish, A. N., Belotelov, V. I. & Zvezdin, A. K. Optical properties of toroidal media. *SPIE Conf. Proc.* **6728,** 67283D (2007).
38. Belotelov, V. I., Bykov, D. A., Doskolovich, L. L., Kalish, A. N. & Zvezdin, A. K. Giant transversal Kerr effect in magnetoplasmonic heterostructures. *J. Exper. Theor. Phys.* **137,** 932–942 (2010).
39. Ebbesen, T. W., Lezec, H. J., Ghaemi, H. F., Thio, T. & Wolff, P. A. Extraordinary optical transmission through sub-wavelength hole arrays. *Nature* **391,** 667–669 (1998).
40. Wood, R. W. Anomalous diffraction gratings. *Phys. Rev.* **48,** 928–936 (1935).
41. Sarrazin, M. & Vigneron, J. P. Bounded modes to the rescue of optical transmission. *Europhys. News* **38,** 27–31 (2007).
42. Luk'yanchuk B. *et al.* The Fano resonance in plasmonic nanostructures and metamaterials. *Nature Mater.* **9,** 707–715 (2010).
43. Porto, J. A., Garcia-Vidal, F. J. & Pendry, J. B. Transmission resonances on metallic gratings with very narrow slits. *Phys. Rev. Lett.* **83,** 2845–2848 (1999).
44. Marquier, F., Greffet, J., Collin, S., Pardo, F. & Pelouard, J. Resonant transmission through a metallic film due to coupled modes. *Opt. Express* **13,** 70–76 (2005).
45. Kimel, A. V., Kirilyuk, A., Tsvetkov, A., Pisarev, R. V. & Rasing, Th. Ultrafast non-thermal control of magnetization by instantaneous photomagnetic pulses. *Nature* **435,** 655–657 (2005).
46. Moharam, M. G., Pommet, D. A., Grann, E. B. & Gaylord, T. K. Stable implementation of the rigorous coupled-wave analysis for surface-relief gratings: enhanced transmittance matrix approach. *J. Opt. Soc. Am. A* **12,** 1077–1086 (1995).
47. Li, L. Fourier modal method for crossed anisotropic gratings with arbitrary permittivity and permeability tensors. *J. Opt. A* **5,** 345–355 (2003).

Acknowledgements

This work was supported by the Deutsche Forschungsgemeinschaft (DFG), the Russian Foundation for Basic Research (RFBR), the Indian Department of Science and Technology (DST) and Russia President's grant (MK-3123.2011.2).

Author contributions

V.I.B. and A.K.Z. conceived and designed the experiments. V.A.K., A.V.G., A.S.V. and S.K. fabricated the sample. V.I.B., I.A.A. and M.P. performed the experiments. V.I.B., A.K.Z. and I.A.A. analysed the data. V.I.B., M.B., A.K.Z., I.A.A. and D.R.Y. co-wrote the paper. All authors discussed the results and commented on the manuscript.

Additional information

The authors declare no competing financial interests. Reprints and permission information is available online at http://www.nature.com/reprints/. Correspondence and requests for materials should be addressed to V.I.B. and I.A.A.